The Astrophysical Journal, 695:999–1005, 2009 April 20 doi:10.1088/0004-637X/695/2/999

HYPERSONIC BUCKSHOT: ASTROPHYSICAL JETS AS HETEROGENEOUS COLLIMATED PLASMOIDS

Kristopher Yirak[1], Adam Frank[1], Andrew J. Cunningham[1,2], and Sorin Mitran[3]
[1] Department of Physics and Astronomy, University of Rochester, Rochester, NY 14620, USA; yirak@pas.rochester.edu
[2] Lawrence Livermore National Laboratory, Livermore, CA 94551, USA
[3] Department of Mathematics, Applied Mathematics Program, University of North Carolina, Chapel Hill, NC 27599, USA
Received 2008 May 30; accepted 2009 January 15; published 2009 April 6

ABSTRACT

Herbig-Haro jets are commonly thought of as homogeneous beams of plasma traveling at hypersonic velocities. Structure within jet beams is often attributed to periodic or "pulsed" variations of conditions at the jet source. Simulations based on this scenario result in knots extending across the jet diameter. Observations and recent high energy density laboratory experiments shed new light on structures below this scale and indicate they may be important for understanding the fundamentals of jet dynamics. In this paper, we offer an alternative to "pulsed" models of protostellar jets. Using direct numerical simulations we explore the possibility that jets are chains of subradial clumps propagating through a moving interclump medium. Our models explore an idealization of this scenario by injecting small ($r < r_{\rm jet}$), dense ($\rho > \rho_{\rm jet}$) spheres embedded in an otherwise smooth interclump jet flow. The spheres are initialized with velocities differing from the jet velocity by ∼15%. We find that the consequences of shifting from homogeneous to heterogeneous flows are significant as clumps interact with each other and with the interclump medium in a variety of ways. Structures which mimic what is expected from pulsed-jet models can form, as can be previously unseen, "subradial" behaviors including backward facing bow shocks and off-axis working surfaces. While these small-scale structures have not been seen before in simulation studies, they are found in high-resolution jet observations. We discuss implications of our simulations for the interpretation of protostellar jets with regard to characterization of knots by a "lifetime" or "velocity history" approach as well as linking observed structures with central engines which produce the jets.

Key words: hydrodynamics – ISM: Herbig-Haro objects – ISM: jets and outflows

1. INTRODUCTION

Herbig-Haro (HH) objects have been the subject of significant analytical, observational, and numerical attention since their discovery. Observations using optical (e.g., Bally et al. 2002) and IR (e.g., Velusamy et al. 2007) techniques reveal that these jets typically show striking large-scale collimation extending out to parsec distances combined with features appearing on a range of smaller scales.

Structure along the jet beam ("knots" or "clumps") has in particular received considerable attention. The origin of knots remains a subject of debate. Early studies focused on clumpyness of the HH bow shocks; Norman & Silk (1979) postulated the existence of single "interstellar bullets," while Schwartz (1978) attributed the structures to stationary clumps being overrun by a wind. Stationary crossing shocks due to an overpressured jet beam expanding and then re-collimating were an early possibility that was considered for knots along the beam (Falle et al. 1987; Bührke et al. 1988; Raga et al. 1990a). More recently, Rubini et al. (2007) have suggested oblique shock focusing as a natural mechanism for hydrodynamic knot formation, though the presence of magnetic fields (Hartigan et al. 2007), precession (Masciadri et al. 2002a), and interactions with the environment (Raga et al. 2002a; de Gouveia Dal Pino 1999; Yirak et al. 2008) all offer other means by which dense clumps might be created.

A large number of studies have attempted to address the question by using a time-dependent launching mechanism (boundary condition). In these simulations typically the density and velocity cross-sectional profiles ($\rho_j(r)$ and $v_j(r)$) are kept fixed, while the magnitude of the velocity varies in some fashion. If the velocity variation is of large enough magnitude, material will pile up enough to form a pair of up- and downstream-facing shocks which travel together and are called "internal working surface." Multiple periods of velocity variation results in multiple internal working surfaces. This "pulsation" model was first proposed by Rees (1978). Currently the most favored model is one in which the variation is sinusoidal; this model was extensively explored by Raga and Collaborators (Raga et al. 1990b; Biro & Raga 1994; Raga & Biro 1993). The pulsation scenario has become so dominant that even when attempting to address questions unrelated to clump formation, periodic inflow variations are frequently employed (e.g., Suttner et al. 1997). Völker et al. (1999) studied the interplay of several different features, including pulsation, opening angle, precession, and radial velocity shear. Other types of pulsation include sawtooth variations (Masciadri et al. 2002b) and step-function variations (de Gouveia Dal Pino & Benz 1994). While most studies employ regular periodicity, Vitorino et al. (2002) investigated a disk/jet launching model in which the velocity was a combination of a fixed and a random component.

A variety of observational signatures can be recovered using sinusoidal pulsed jet models through careful choice of specific jet physical parameters and sinusoidal variability. In Raga et al. (2002b), for example, a two-mode launching model was proposed using velocity histories extracted from observations of HH 34 and HH 111. Using these pulsation modes axisymmetric hydrodynamic simulations provided a convincing match to the location of the leading bow shock and the location of bright knots in the beam. These and similar results provide strong support for pulsed jet models.

A detailed examination of jets observed at the highest spatial resolution however shows features which do not fit into the pulsed jet paradigm. In particular, a number of "archetypal" jets show features at scales below the jet radius ($r < r_j$) which are distinctly displaced from the jet axis. In the case of HH 47, the jet

clearly shows a nonaxisymmetric morphology in the form of an apparent helical bending of the beam (Hartigan et al. 2005). The beam itself is defined by a sequence of quasi-periodic knots with displacements to either side of the nominal jet axis. Explanations for this bending have included impacts with objects (Raga et al. 2002a; de Gouveia Dal Pino 1999), magnetic fields (Hartigan et al. 2007), and precession of the jet source (Masciadri et al. 2002a). We consider the presence of subradial, nonaxisymmetric features to be a challenge to the pulsed jet paradigm. Here, we consider an alternative to the pulsed jet model and investigate the consequences of intrinsic density heterogeneity in jet formation and evolution.

We note that we are motivated to explore this model both by observations and new high energy density laboratory astrophysics (HEDLA) plasma experiments. Using pulsed power wire array technologies, Lebedev et al. (2005) and Ciardi et al. (2007, 2009) have presented experiments that track the evolution of fully magnetized, hypersonic, radiative jets. The stability of hydro and magnetohydrodynamics (MHD) jets has long been a topic of debate, and these experiments shed some light on the real dynamics of three-dimensional systems (Xu et al. 2000). The experiments show that kink mode instabilities strongly affect the jet. As the kink mode grows into the nonlinear regime its disrupts but does not destroy the jet. The saturation of the instability rapidly transforms the jet into a sequence of collimated chains of knots which propagate with a range of velocities. Similar fragmented chains have been seen in other pulsed power experiments (Golingo et al. 2005). In the last section of the paper, we discuss some possible mechanisms by which subradial knots are created in jets.

Thus, we propose a model in which the velocity and density profile of the jet are variable in time and space on scales less than the jet age and jet radius, respectively. Specifying conditions on these scales allows the model to achieve complex structures not seen before in simulations. Our simulations utilize adaptive mesh refinement (AMR) techniques and so are able to resolve clumps in the jet beam at acceptable levels.

In the following sections, we describe the model in detail, offer dynamical and observational signatures, and briefly discuss the results.

2. COMPUTATIONAL METHOD AND PHYSICAL MODEL

Numerical simulations were undertaken with the *AstroBEAR* computational code.[4] *AstroBEAR* is a parallel AMR code which allows a variety of choices for numerical solvers, integration schemes, and cooling modules for hydrodynamic or MHD astrophysical fluids (Cunningham et al. 2006, 2009). Here, the code solved the three-dimensional hyperbolic system of equations for inviscid, compressible flow using a spatial second-order and temporal first-order accurate Monotone Upwind-Centered Scheme for Conservation Laws (MUSCL) using a Roe-averaged linearized Riemann solver. Simple radiative cooling is included separately using an iterative source term with the cooling curve of Dalgarno & Mccray (1972).

In what follows, the geometry of the system is taken to have the jet axis aligned with the z-axis, with x- and y-axes following the right-handed convention. A base grid of $36 \times 36 \times 96$ cells covered the simulation domain of extent $1200 \times 1200 \times 3200$ AU. *AstroBEAR* employs a patch-based adaptive grid to refine areas of interest; here, two levels of refinement were used, yielding a maximum effective resolution of $288 \times 288 \times 768$ cells. This corresponds to a minimum cell length of $\Delta x = 6.23 \times 10^{13}$ cm ($\sim$4 AU). All boundaries had outflow conditions, with user-specified conditions in the jet launching region.

The ambient number density and temperature were initialized to constant values of $\rho_a = 10$ cm^{-3} and $T_a = 2000$ K, respectively, giving a sound speed of $c_a = 5.26$ km s^{-1}. The inhomogeneities in the beam were introduced as spherical density and velocity perturbations in an otherwise smooth beam: we shall refer to the former as "clumps" and the latter as "jet." The jet had number density, radius, velocity, and temperature of $\rho_j = 10^2$ cm^{-3}, $r_j = 100$ AU, $v_j = 150$ km s^{-1}, and $T_j = 2000$ K. This resulted in a Mach 30, overdense ($\chi_{ja} \equiv \rho_j/\rho_a = 10$), and overpressured ($p_j/p_a = 10$) jet. The jet was launched at $x, y = 600$ AU on the $z = 0$ plane. The clumps all had the same initial number density of $\rho_c = 10^3$ cm^{-3}, yielding density ratios of $\chi_{cj} \equiv \rho_c/\rho_j = 10$ and $\chi_{ca} \equiv \rho_c/\rho_a = 10^2$. The clumps were seeded with radii and velocities that were random within ranges of $r_c = 26$–60 AU, and $v_c = 132$–168 km s^{-1}. Relative to the jet, these correspond to ranges $r_c/r_j = 0.26$–0.60 and $v_c/v_j = 0.88$–1.12. The x and y locations of the clumps in the jet were random with the constraint that the entire clump be located within the jet beam. All clumps were seeded at the same z location in the grid. The clumps had temperatures such that they were in pressure balance with the jet beam (assuming a relative velocity of zero). They were seeded 8 yr apart; this resulted in the production of 12 clumps before the end of the simulation ($t_{\rm sim} = 100$ yr).

At the maximum AMR level, the jet radius was resolved by 24 cells, and the clump radii by 6–14 cells. This represents probably the lower limit on desirable resolution. Jet, clump, and ambient materials were separately tracked with passive advected tracers.

3. RESULTS AND ANALYSIS

A time sequence of the simulation is given over four panels in Figure 1. Density plots and a Schlieren image are shown in Figure 2. Figure 1 shows a three-dimensional representation of the simulation in the form of a set of isodensity contours. In the panels, the jet beam enters from the left-hand side of the grid and propagates to the right. Shortly after the start of the simulation, knots appear with random sizes, locations, and speeds. The figure has been adjusted to track the evolution of the clumps via an isodensity contour of a passive clump tracer (in green). Thus, the clumps are readily recognizable as initially spherical inclusions within the beam close to the inflow boundary cells. As the simulation progresses, the clumps evolve via their interaction with the interclump material in the beam and, in some cases, with other clumps.

We note that bow shocks form for clumps with high enough differential speeds relative to the beam, i.e., $|\Delta v_c| = |v_c - v_j| > c_j$, where c_j is the sound speed in the jet beam. As a bow shock propagates into the beam material, a transmitted shock will propagate into and compress the clumps. If the differential velocity $\delta v_c = \Delta v_c/v_j$ is positive then the bow shock faces forward into the direction of jet propagation. If δv_c is negative then the bow shock will face backward toward the jet source. These bow shocks are not directly visible in Figure 1; however, the sign of δv_c is apparent in the compression occurring on the leading (trailing) edges when δv_c is positive (negative). The bow shocks are apparent in Figure 2. In the bottom panel, the clump at $z = 2100$ AU has $\delta v_c > 0$ and hence a forward facing shock forms at its leading edge while the larger clump at $z = 900$ AU shows the opposite behavior. We note also the

[4] Information about the *AstroBEAR* code may be found online, at http://www.pas.rochester.edu/~bearclaw/

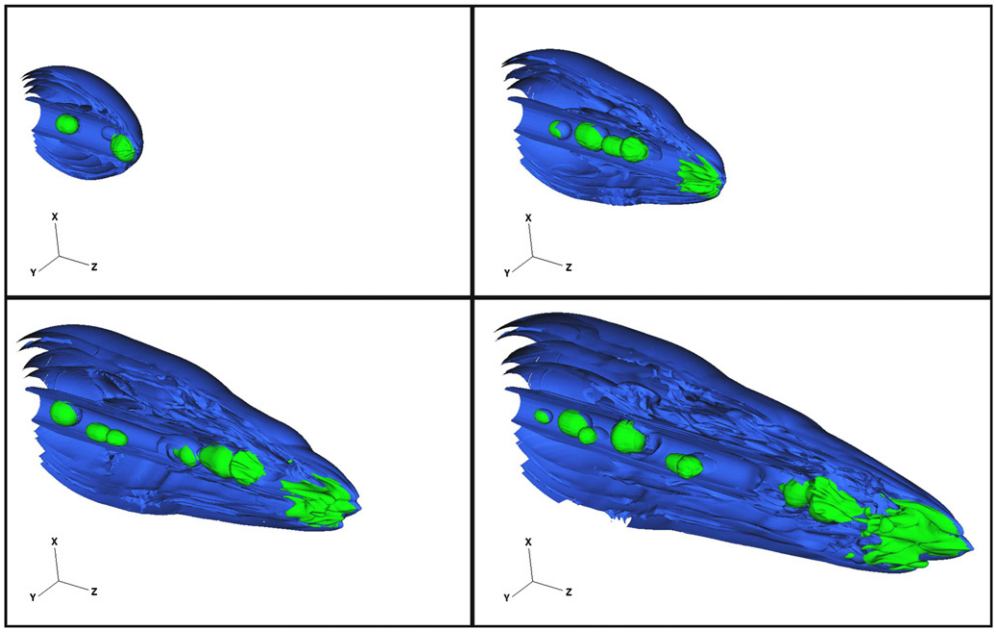

Figure 1. Isocontours of logarithmic density at four times in the simulation, $t = 30$, 53, 77, and 100 yr. The clumps are depicted in light green, with the jet material in blue. The x–z plane along the jet axis clips the jet material contours.

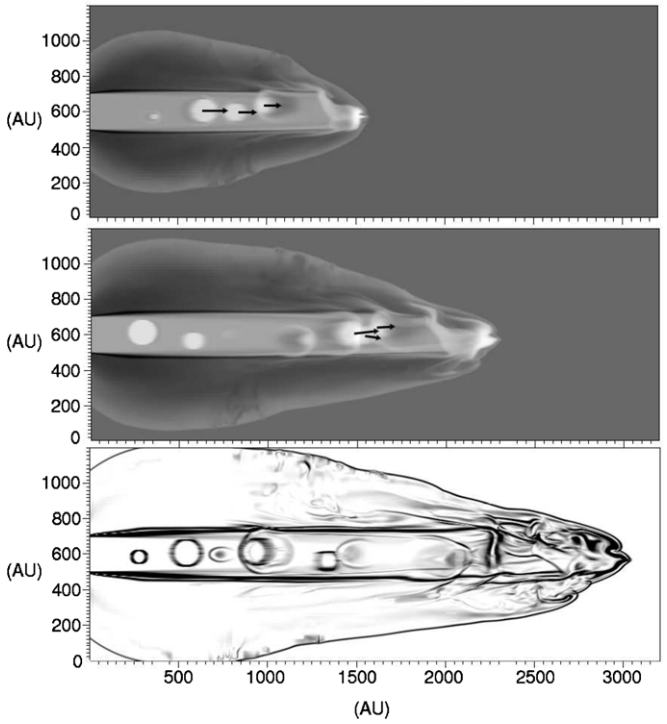

Figure 2. Top two panels give gray-scale images of logarithmic density in the x–z plane located on the jet axis at two different times, $t = 53$ and 77 yr, corresponding to the lower left and upper right panels of Figure 1. Lighter gray corresponds to denser material. Velocity vectors originating at three knots have been overlaid, and they are seen to change as the knots interact. Bottom panel shows a synthetic Schlieren image at $t = 100$ yr, which illuminates such features as a clump with a forward bow shock at $z = 2100$ AU, a clump with reverse bow shock at $z = 900$ AU, and clump-induced "spur shocks" at several places along the jet beam. The disklike feature at $z = 2300$ AU is discussed further in the text.

presence of "spur shocks" in the bottom panel of Figure 2. These are concave shocks that originate at the edges of the beam and arc away from the beam (Heathcote et al. 1996). We find that the presence of clumps off-axis naturally leads to the development of such structures.

Once clumps are launched into the jet there are three possible consequences. The first consequence is the clump propagating downstream unimpeded and colliding with the jet head. In this case the dense clump may break through the bow shock defining the front edge of the jet, leading to significant nonaxisymmetric structures there. This behavior is apparent in both Figures 1 and 2 where a dense clump has already traversed the jet length and propagated through the jet shock/bow shock structure at the terminus of the beam. The presence of a significant "knob" protruding at the lower edge of the jet head defines the extent of the clump which now forms at the leading edge of the jet.

A second possibility however is that the clump will not make it to the leading edge of the jet. The behavior of shocked clumps has been extensively studied both analytically and numerically (e.g., Klein et al. 1994; Jones et al. 1996; Poludnenko et al. 2002; Fragile et al. 2004). These studies demonstrate that a clump compressed by a strong transmitted shock wave (in this case the transmitted wave originates from its relative motion within the beam) will eventually be destroyed in a "cloud crushing time" given approximately by $t_{cc} = 2r_c\chi_{cj}^{1/2}/|\Delta v_c|$, where $\chi_{cj} = \rho_c/\rho_j$. If this happens before the clump reaches the jet head then the clump material will be dispersed within the beam. Thus the cloud crushing timescale should be compared with the timescale required to cross the length of the jet beam, $t_{jc} = L_j/(v_c - v_{bs})$. Note that $L_j = v_{bs}t$, where v_{bs} is the speed of the jet head given by the familiar formula $v_{bs} = v_j(1 + \chi_{ja}^{-1})^{-1/2}$ and t is the time at which the clump is launched. Comparing these expressions we find the critical launching time t^*,

$$t^* = \frac{2r_c}{|\Delta v_c|}\sqrt{\chi_{cj}}\left(\frac{v_c}{v_j}\sqrt{1+\chi_{ja}^{-1}} - 1\right) \quad (v_c \neq v_j). \qquad (1)$$

A clump of radius r_c, velocity dispersion Δv_c, and density ratio χ_{cj} needs to be launched at a time $t = t_{\rm launch} < t^*$ in order for it to reach the jet head before being destroyed. For each instantiated

clump, comparing $t_{\rm launch}$ to t^* reveals that $t_{\rm launch} < t^*$ for three of the 12 clumps. This implies that late in time (assuming no other interactions) nine of the 12 clumps would disperse before reaching the jet head. However, $t_{cc} > t_{\rm sim}$ for all the clumps in the simulation ($t_{\rm sim}$ is the duration of the simulation). We therefore expect all clumps to exert a strong influence on the jet beam throughout the simulation, and we expect some of the clumps to affect strongly the morphology of the jet head. These expectations are confirmed in the simulation.

The third possibility for the long-term evolution of a clump, assuming δv_c is not the same for all clumps, is interaction with another clump. The interaction can take the form of direct or glancing collision depending on the impact parameter b. Even when $b > 2r_c$ there can still be interactions between a clump-driven bow shock and a neighboring clump (Poludnenko et al. 2002). Such interactions will be determined by the width of the clump bow shock which will, in general, be determined by the Mach number of the clump through the interclump beam media ($M_c = |\Delta v_c|/c_j$). The collisions of clumps are also a process which has been well studied, and one expects the formation of transmitted shock waves within the clumps which heat and compress clump material as it streams into the shock (Klein et al. 1994; Miniati et al. 1999). Figures 1 and 2 show a number of such interactions occurring. By the last panel of Figure 1, clump collisions have resulted in a merged structure near the head of the jet, and their effect on each other and on the jet beam itself is complex. It is noteworthy however that the collision, compression, and subsequent merger of clumps can come to resemble the internal working surfaces in homogeneous pulsed jets. Note the resemblance in the bottom panel of Figure 2 of the structure at $z = 2300$ AU to the thin shock bounded working surfaces seen in jet pulsation simulations. An important difference in the case of clumps however is that these structures remain subradial. The merged structure identified at $z = 2300$ AU has a lateral width of $h \approx 1.8r_j$ and is offset from the jet axis by $r_0 \approx 0.25r_j$. Thus, even collisions between slow moving clumps overtaken by faster moving ones differ from what is expected for homogeneous jet beams with varying inflow velocity. In this case, the resulting shock structures are slightly smaller than the jet diameter and displaced from the jet axis.

The difference between homogeneity and heterogeneity is particularly striking for glancing clump collisions: $r_c < b < 2r_c$. In these cases, the clump–clump interaction will be off center and one can expect from momentum conservation that nonaxial motions will result. The top two panels of Figure 2 illustrate this point, showing the off-center collision of three clumps. Before the collision the velocity vectors of all three clumps are purely axial $\vec{v} = v_z\hat{e}_z$. After the collision the clumps have acquired transverse v_r velocities. The ability to generate nonaxial motions within the beam via clump interactions is an important point as proper motion studies of highly resolved HH jets show knot-to-knot variability in both direction and speed (Hartigan et al. 2005; Bally et al. 2002). Moreover, this interaction forms the structure at $z = 2300$ AU seen in the bottom panel of Figure 2 which therefore has varying velocity components across its surface, in contrast to similar structures in pulsed-jet models.

We note again that the clump injection time, position within beam cross section, and velocity were all chosen randomly within constraints.

We now address the issue of the observational properties of jets with this kind of heterogeneity, with respect to assumptions of pulsation. In many studies lifetimes of features along an HH beam jet beam are derived by relating the current position of the feature and its proper motion (Bally et al. 2002; Hartigan et al. 2005). Going a step further several some studies (e.g., Raga & Noriega-Crespo 1998; Raga et al. 2002b)) infer full velocity histories of jets from observations in terms of multiple pulsation modes at the jet launch region. While these studies are able to convincingly reproduce some observational characteristics of the jets, our models of heterogeneous jets shed new light on the issue of recovering pulsation histories from observations. We note that inferring ejection histories from current positions and velocities requires two intrinsic assumptions: first, that the launching is smoothly varying and periodic in nature, and second, that pulsation-formed knots are coherent throughout their lifetimes. In particular, it is assumed that given a position z_0 for a hypersonic, semiballistic jet, the time variability in the past can be inferred from the current observed velocity structure. Considering the current epoch to be $t = 0$ one uses observed axial velocity $v(z_0)$ to compute dynamical times $t_0 = -z_0/v(z_0)$ for fluid parcels when they were ejected from the source. The velocity history of the jet as $v_j(t) = v\,[t = -z/v(z)]$ can then be derived. In Raga et al. (2002b) for HH 34 and HH 111 it was assumed that $v_j(t)$ could be described by a periodic function of the form

$$v_j(t) = v_{j,0} + \sum_{k=1}^{n} v_j^{(k)} \sin\left(\frac{2\pi t}{\tau_k} + \phi_k\right), \qquad (2)$$

where $v_j^{(k)}$, τ_k, and ϕ_k are the amplitude, period, and phase of each pulsation mode. For HH 111, $n = 1$, while for HH 34, accounting for the collimated knots near the source requires $n = 3$.

Assuming Equation (2) for $v_j(t)$ can bias the description of jets as we now demonstrate. For each data frame in our simulation, we may perform a similar analysis; see Figure 3. Along the axis of the jet we may denote the locations of "knots" as those positions where the density peaks at some value above the jet density. The axial density profile is given in the left panel of Figure 3, with knots identified by circles. We then take the velocities at these positions to be the knot velocities. This allows us to calculate dynamical times and, using a single mode ($n = 1$) for simplicity, reconstruct a separate velocity history for each data frame in the simulation.

As implied by the second assumption above, in order for this analysis to be valid the resulting amplitude and period should be robust to the time in the simulation, especially late in time when there are the greatest number of knots. We found that the results were not robust, as depicted in the right-hand panels of Figure 3. The three panels show, from top to bottom, the result of least-squares fits to the data at $t = 100$, 80, and 40 yr with 1σ error bounds overlaid. The top panel shows the fit resulting from the corresponding data given in the left panel. The average velocity of the knots remains roughly constant for each of the three times depicted and is close to the jet velocity ($v_j = 150$ km s^{-1}), as expected. However, the amplitude varies by ~30% over time, and the period varies by over 100%. The goodness of the fits, though less at $t = 80$ yr than the other two times depicted, appears adequate. Although not explicitly shown here, variation in the fit results shows correlation with knot–knot interactions.

4. DISCUSSION AND CONCLUSIONS

We have performed three-dimensional simulations using a new "collimated clumps" scenario for protostellar jets. Our

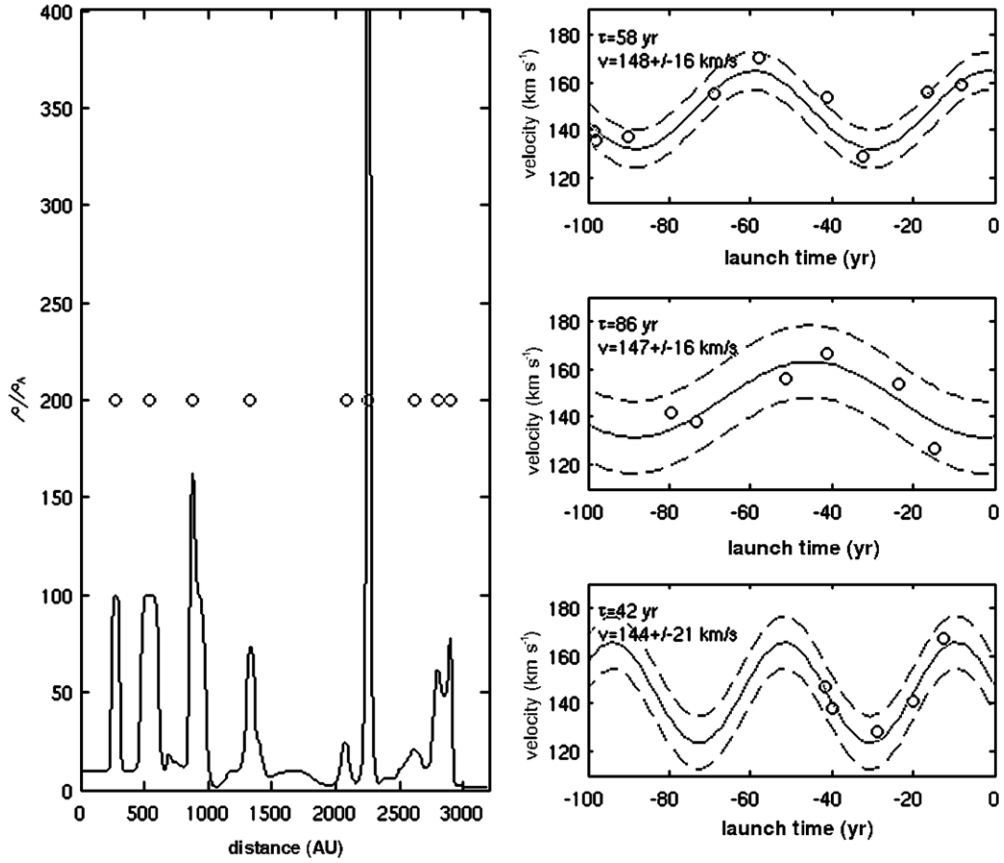

Figure 3. (Left panel) Axial density profile normalized by the ambient density, ρ/ρ_a, is plotted with positions designated as "knots" given by "$\circ$." (Right panels) From top to bottom, velocities for knots ("$\circ$") vs. their launching (dynamical) time at t =100, 80, and 40 yr. Results from least-squares fits are shown with 1σ error overlaid. The period τ and mean velocity with single-mode sinusoidal amplitude, $v_j = v_{j,0} \pm v_j^{(1)}$, are printed on each panel.

model offers a fundamentally different paradigm for understanding jet origins and dynamics in the sense that heterogeneity is seen as being intrinsic and links the jet morphology on "mesoscales" to the processes (such as instabilities) occurring on "microscales" near the central engine.

While the pulsed-jet model has been successful at interpreting some aspects of jets, it may be misleading if used too generally. In particular, the assumption of sinusoidal pulsations can limit the interpretation of HH object observations. In our simulations, which had no sinusoidal variation in time, we nonetheless were able to recover (erroneous) sinusoidal behavior using an analysis similar to that which has been carried out in the past on observations. While one part of this behavior (the mean velocity $v_{j,0}$) fits the initial conditions well, the assumption of periodic pulsation allows the false conclusion that the structures in the beam arose due to periodic ejection behavior. We conclude therefore that care should be taken when attributing observations of apparent sinusoidal velocity in protostellar jets to corresponding sinusoidal behavior of a central engine.

A common thread in pulsed-jet models is the lack of radial variation within the jet beam—that is, at the boundary $v(r, t) = v(t)$ and $\rho(r, t) = \rho(t)$ for $r < r_j$. This is a result of both an intentional simplifying assumption and computational limitations. Thus in future studies it would be of interest to re-examine pulsed simulations with this constraint relaxed.

In contrast to pulsed-jet models, our model offers two attractive features: first, a natural mechanism (knot–knot interactions) helps explain small-scale features along the jet axis. The idea that knots or bow shocks in HH objects are evolving clumpy structures has been discussed before in the context of observations (e.g., Reipurth et al. 2002), with ongoing *Hubble Space Telescope* (*HST*) observations giving continued support to this idea (e.g., Hartigan et al. 2005). The interaction of distinct subradial knots with each other and with an overall bow shock offers a simple explanation for such evolution. The second feature the model offers is the presence of unique observational characteristics in the form of forward- and reverse-facing bow shocks and spur shocks at the edges of the jet beam. Our scenario provides a simple mechanism for the formation of subradial nonaxisymmetric features via multiple dense, clumps which have a nonzero velocity dispersion. The ease with which nonaxisymmetric features like spur shocks (Heathcote et al. 1996) develop in our models is attractive.

We note that reverse-facing bow shocks are far less common in observations than forward-facing bow shocks. Bally et al. (2002) gave a few examples in the HH 2 bow shock. Knot U in HH 2 is an off-axis, backward-facing bow shock feature. Owing to its low proper motion ($\sim$30 km s^{-1} vs. $>$ 100 km s^{-1} elsewhere), it was interpreted as a small, dense clump being overrun by the HH 2 bow shock. We recall that in our model, both forward- and backward-facing bow shocks will propagate *along* with the jet. Backward-facing bow shocks will travel upstream only in the jet rest frame. Thus, the distance between a backward-facing bow shock and the launching engine, as well as the distance between a backward-facing bow shock and the

leading jet bow shock, will increase over time. This is in general agreement with the behavior exhibited by knot U.

Features resulting from collisions of forward- and reverse-facing bow shocks, such as that shown in the bottom panel of Figure 2, should have a complex evolution. In particular, the velocity profile transverse to the propagation of the jet would be more complex than in a unperturbed clump (or than in the internal working surface of a pulsed jet). It is useful to note that it has been observed that peaks in emission of knots do not necessarily correspond to peaks in velocity, see e.g. Riera et al. (2003) for HH 110 and Riera et al. (2001) for HH 111, owing perhaps to the three-dimensional nature of the knots.

The clump destruction mechanisms are the same for forward- or backward-facing clumps. Therefore, we would expect their numbers as a function of distance from the source to be about equal (assuming the two populations of faster-than-jet and slower-than-jet clumps have equal number and average relative velocities). The fact that so few reverse-facing bow shocks are found observationally helps constrain the model by suggesting a bias of clump velocities toward values greater than the jet beam velocity. At the limits of our parameter space however we note that it is possible that no jet beam exists at all and what is observed is material left in the wake of clump–clump collisions

We now address the issue of the origin of clumps within jets. Since our model posits a disrupted but comoving cohort of clumps, we therefore look to the jet launching as a viable means of producing such a supersonic, knotted jet. We will address instabilities that can occur further downstream below. Ouyed et al. (2003) discussed in detail magnetized jet launching from Keplerian disks. In particular, they find that the jet is unstable to magnetic column instabilities near the source, when the flow has propagated far enough to become super-Alfvénic. The jet is not completely disrupted, however, owing to self-limiting processes which serve to keep the Alfvénic Mach number of order unity as the jet propagates. This is in general agreement with the results of Hartigan et al. (2007). In that work the authors demonstrate that in stellar jets the Alfvén velocity decreases with distance from the source. Hence, it is only close to the launching region that the jets are believed to be unstable to magnetic instabilities. Since it would be computationally unfeasible to track the evolution of a jet from the source out to the scales presented here,[5] we choose to take the "clumpyness" of the jet as a boundary condition.

We note that the general issues of the stability of jets particularly at "microscale" regions near the launch region remain unresolved (Königl 2004; Ouyed et al. 2003; Xu et al. 2000; Micono et al. 1998). In addition, the issues of magnetic field strength and velocity perturbations near the jet launch region also present problems (Hartigan et al. 2007) as noted above. Although we do not explicitly consider details of disk/jet launching in this study, plausible scenarios present themselves. It has long been considered that the interaction between the forming star and accretion disk—via magnetic fields—is responsible for jet launching (Königl 1982). Further, anisotropy of the magnetized disk during the young stellar object (YSO) phase is a distinct possibility, as suggested by Combet & Ferreira (2008). One could therefore theorize, for example, noncylindrically symmetric accretion bursts as a driver for nonaxial density enhancements in the jet beam. As to the regular period between clumps, this assumption seems reasonable in light of the work of Vitorino et al. (2002). That work postulated random launching velocity components, which nonetheless ended up forming a quasi-periodic jet structure.

Recent HEDLA investigations provide a unique window into the behavior of fully three-dimensional radiative hypersonic MHD jets. These experiments demonstrate that magnetized jet beams in the lab may rapidly break up into a sequence of quasi-periodic knots due to current-driven instabilities (Ciardi et al. 2007, 2009). These knots may be displaced from the nominal jet axis and may propagate with varying velocities. This results in morphologies qualitatively reminiscent of HH-jet beams. It should be noted that the present simulation does not employ magnetic fields; however, it remains an open question whether magnetic fields remain dynamically important on the length scales of consideration here (Hartigan et al. 2007; Ostriker et al. 2001). It seems plausible that a process similar to what was observed in the lab could occur in the astrophysical context, beginning with a beam close to the central engine which becomes disrupted owing to the kink and sausage instabilities on small to intermediate scales. This would result in a series of knots which continue to evolve as they propagate away from the central engine. Such a scenario would also explain the observed velocity differences between knots, attributable to the particulars of each knot's formation. The present simulation is an idealization of this model.

We note that nonaxial features may also be obtained by assuming a precessing launching engine. Masciadri et al. (2002a), for example, sought to model the HH 34 system with a precessing jet with time-dependent launching, in three dimensional. They found that, depending on the time of observation, the emission structure varied considerably, as would be the case with the present model. However, an inherent aspect of a precessing source is nonaxially aligned velocity vectors of the knots (see, e.g., Figure 6 of Masciadri et al. 2002a). In contrast, in HH 111 while some of the knots are displaced from the axis of the jet, the velocity vectors overall appear well aligned with the outflow axis (see, e.g., Figure 1 of Hartigan et al. 2001). We note that strong toroidal velocity components (e.g., Cerqueira et al. 2006) would further complicate the issue.

Turning to generic instabilities in the jet beam as the source of clumps, previous studies have shown that adiabatic or radiatively cooling jet beams are susceptible to instabilities in both magnetized and unmagnetized cases (e.g., Thiele & Camenzind 2002; de Gouveia Dal Pino & Benz 1993). For a highly supersonic, overdense (hence, overpressured) jet as we have here ($M = 30$ both internally and externally), a steady jet beam should not be susceptible to disruption from surface KH modes (e.g., Payne & Cohn 1985). Conversely, while reflection modes exist for any supersonic beam, they also are not seen to disrupt a highly supersonic beam (e.g., Payne & Cohn 1985). Moreover, it has been argued that emission from these modes could not correspond to the observed knots in HH objects: unless magnetic fields are dynamically important, the derived knot spacing (i.e., the pattern wavelength) is higher than typical interknot distances in HH objects (Thiele & Camenzind 2002).

In this study, we have not explicitly considered the interaction between jet beam reflection modes and the clumps. The presence of the jet beam itself is a constraint which could be removed, resulting in a host of clumps with no jet (hence, no internal

[5] To illustrate the difficulty, we note that two numerical studies which have attempted this are Hartigan et al. (2007) and Masciadri et al. (2002a). The former employed cylindrical symmetry (instead of three dimensional), while the latter employed an AMR scheme which refined maximally only in regions near the source (see Figure 1 of that work). Though the jet radius increased quickly with distance from the boundary, at the boundary at the maximum resolution there were ∼1.5 cells per jet radius.

modes except those excited within the clumps themselves). We note for completeness that clumps moving subsonically relative to the jet beam will form a bow wave instead of a bow shock and should be more susceptible to disruption by KH instabilities; however, this was the case for only four of the instantiated clumps. Additionally, the ability of this model to reproduce the observed emission of HH objects is very important. We are presently working to implement the ability to generate synthetic emission maps from *AstroBEAR* simulations.

The degree to which the results of the simulation presented here depend on the values chosen for parameters such as χ_{cj} and Δv_c requires further investigation. In particular, $t_{\rm launch} < t^*$ was not satisfied for all of the instantiated clumps, implying that some should disperse before reaching the jet head. The present simulation did not progress far enough to witness this behavior (that is, $t_{cc} > t_{\rm sim}$). Also, using a $\Delta v_c \neq 0$ and varying from clump to clump should result in an injection of considerable vorticity into the jet beam. Future work should therefore explore the long-term evolution of the clumped jet. The aspect ratio (length/width) of the jet's final state in the present simulation is less than that for HH objects, implying again that simulations which progress for longer times would be of interest. While increased resolution would of course be of benefit, extracting details of clump–clump interaction within the jet-beam environment is probably outside the scope of this study and would be appropriate for a separate investigation (T. Dennis et al. 2008, in preparation). Finally, the inclusion of magnetic fields to study scenarios of knot formation and the resulting observational consequences would be of additional interest.

We thank the referee, Elisabete de Gouveia Dal Pino, for her insightful comments and questions. This manuscript is improved and clarified as a result of her review. We would like to thank Pat Hartigan, Sergey Lebedev, and Andrea Ciardi for their time. Tim Dennis and Brandon Shroyer also provided invaluable support and help.

Support for this work was in part provided by NASA through awards issued by JPL/Caltech through Spitzer program 20269 and 051080-001, the National Science Foundation through grants AST-0507519 as well as the Space Telescope Science Institute through grants HST-AR-10972, HST-AR-11250, and HST-AR-11252. We also thank the University of Rochester Laboratory for Laser Energetics and funds received through the DOE Cooperative Agreement no. DE-FC03-02NA00057.

REFERENCES

Bally, J., Heathcote, S., Reipurth, B., Morse, J., Hartigan, P., & Schwartz, R. 2002, AJ, 123, 2627
Biro, S., & Raga, A. C. 1994, ApJ, 434, 221
Bührke, T., Mundt, R., & Ray, T. P. 1988, A&A, 200, 99
Cerqueira, A. H., Velázquez, P. F., Raga, A. C., Vasconcelos, M. J., & de Colle, F. 2006, A&A, 448, 231
Ciardi, A., et al. 2007, Phys. Plasmas, 14, 6501
Ciardi, A., et al. 2009, ApJ, 691, L147
Combet, C., & Ferreira, J. 2008, A&A, 479, 481
Cunningham, A. J., Frank, A., & Blackman, E. G. 2006, ApJ, 646, 1059
Cunningham, A. J., Frank, A., Carroll, J., Blackman, E. G., & Quillen, A. C. 2009, ApJ, 692, 816
Dalgarno, A., & Mccray, R. A. 1972, ARA&A, 10, 375
de Gouveia Dal Pino, E. M. 1999, ApJ, 526, 862
de Gouveia Dal Pino, E. M., & Benz, W. 1993, ApJ, 410, 686
de Gouveia Dal Pino, E. M., & Benz, W. 1994, ApJ, 435, 261
Falle, S. A. E. G., Innes, D. E., & Wilson, M. J. 1987, MNRAS, 225, 741
Fragile, C. P., Murray, S. D., Anninos, P., & van Breugel, W. 2004, ApJ, 604, 74
Golingo, R. P., Shumlak, U., & Nelson, B. A. 2005, Phys. Plasmas, 12, 062505-1
Hartigan, P., Frank, A., Varniére, P., & Blackman, E. G. 2007, ApJ, 661, 910
Hartigan, P., Heathcote, S., Morse, J. A., Reipurth, B., & Bally, J. 2005, AJ, 130, 2197
Hartigan, P., Morse, J. A., Reipurth, B., Heathcote, S., & Bally, J. 2001, ApJ, 559, L157
Heathcote, S., Morse, J. A., Hartigan, P., Reipurth, B., Schwartz, R. D., Bally, J., & Stone, J. M. 1996, AJ, 112, 1141
Jones, T. W., Ryu, D., & Tregillis, I. L. 1996, ApJ, 473, 365
Klein, R. I., Mckee, C. F., & Colella, P. 1994, ApJ, 420, 213
Königl, A. 1982, ApJ, 261, 115
Königl, A. 2004, ApJ, 617, 1267
Lebedev, S. V., et al. 2005, MNRAS, 361, 97
Masciadri, E., de Gouveia Dal Pino, E. M., Raga, A. C., & Noriega-Crespo, A. 2002a, ApJ, 580, 950
Masciadri, E., Velázquez, P. F., Raga, A. C., Cantó, J., & Noriega-Crespo, A. 2002b, ApJ, 573, 260
Micono, M., Massaglia, S., Bodo, G., Rossi, P., & Ferrari, A. 1998, A&A, 333, 1001
Miniati, F., Jones, T. W., & Ryu, D. 1999, ApJ, 517, 242
Norman, C., & Silk, J. 1979, ApJ, 228, 197
Ostriker, E. C., Stone, J. M., & Gammie, C. F. 2001, ApJ, 546, 980
Ouyed, R., Clarke, D. A., & Pudritz, R. E. 2003, ApJ, 582, 292
Payne, D. G., & Cohn, H. 1985, ApJ, 291, 655
Poludnenko, A. Y., Frank, A., & Blackman, E. G. 2002, ApJ, 576, 832
Raga, A. C., Binette, L., & Canto, J. 1990a, ApJ, 360, 612
Raga, A. C., Binette, L., Canto, J., & Calvet, N. 1990b, ApJ, 364, 601
Raga, A. C., & Biro, S. 1993, MNRAS, 264, 758
Raga, A. C., de Gouveia Dal Pino, E. M., Noriega-Crespo, A., Mininni, P. D., & Velázquez, P. F. 2002a, A&A, 392, 267
Raga, A., & Noriega-Crespo, A. 1998, AJ, 116, 2943
Raga, A. C., Velázquez, P. F., Cantó, J., & Masciadri, E. 2002b, A&A, 395, 647
Rees, M. J. 1978, MNRAS, 184, 61
Reipurth, B., Heathcote, S., Morse, J., Hartigan, P., & Bally, J. 2002, AJ, 123, 362
Riera, A., López, R., Raga, A. C., Anglada, G., & Estalella, R. 2001, RevMexAA, 37, 147
Riera, A., López, R., Raga, A. C., Estalella, R., & Anglada, G. 2003, A&A, 400, 213
Rubini, F., Lorusso, S., Del Zanna, L., & Bacciotti, F. 2007, A&A, 472, 855
Schwartz, R. D. 1978, ApJ, 223, 884
Suttner, G., Smith, M. D., Yorke, H. W., & Zinnecker, H. 1997, A&A, 318, 595
Thiele, M., & Camenzind, M. 2002, A&A, 381, L53
Velusamy, T., Langer, W. D., & Marsh, K. A. 2007, ApJ, 668, L159
Vitorino, B. F., Jatenco-Pereira, V., & Opher, R. 2002, A&A, 384, 329
Völker, R., Smith, M. D., Suttner, G., & Yorke, H. W. 1999, A&A, 343, 953
Xu, J., Hardee, P. E., & Stone, J. M. 2000, ApJ, 543, 161
Yirak, K., Frank, A., Cunningham, A., & Mitran, S. 2008, ApJ, 672, 996